International Journal of Pharmaceutics 408 (2011) 130–137

Contents lists available at ScienceDirect

International Journal of Pharmaceutics

journal homepage: www.elsevier.com/locate/ijpharm

Pharmaceutical Nanotechnology

Novel magnetic iron oxide nanoparticles coated with poly(ethylene imine)-*g*-poly(ethylene glycol) for potential biomedical application: Synthesis, stability, cytotoxicity and MR imaging

Christoph Schweiger[a], Clemens Pietzonka[b], Johannes Heverhagen[c], Thomas Kissel[a,*]

[a] Department of Pharmaceutics and Biopharmacy, Philipps-Universität Marburg, Ketzerbach 63, 35037 Marburg, Germany
[b] Department of Chemistry, Philipps-Universität Marburg, Hans-Meerwein-Straße, 35032 Marburg, Germany
[c] Department of Diagnostic Radiology, Philipps-Universität Marburg, Baldingerstraße, 35043 Marburg, Germany

ARTICLE INFO

Article history:
Received 12 August 2010
Received in revised form 8 December 2010
Accepted 12 December 2010
Available online 18 February 2011

Keywords:
Iron oxide nanoparticles
Poly(ethylene imine)
Poly(ethylene glycol)
Colloidal stability
Cytotoxicity
Magnetic resonance imaging

ABSTRACT

Magnetic iron oxide nanoparticles have found application as contrast agents for magnetic resonance imaging (MRI) and as switchable drug delivery vehicles. Their stabilization as colloidal carriers remains a challenge. The potential of poly(ethylene imine)-*g*-poly(ethylene glycol) (PEGPEI) as stabilizer for iron oxide (γ-Fe_2O_3) nanoparticles was studied in comparison to branched poly(ethylene imine) (PEI). Carrier systems consisting of γ-Fe_2O_3–PEI and γ-Fe_2O_3–PEGPEI were prepared and characterized regarding their physicochemical properties including magnetic resonance relaxometry. Colloidal stability of the formulations was tested in several media and cytotoxic effects in adenocarcinomic epithelial cells were investigated.

Synthesized γ-Fe_2O_3 cores showed superparamagnetism and high degree of crystallinity. Diameters of polymer-coated nanoparticles γ-Fe_2O_3–PEI and γ-Fe_2O_3–PEGPEI were found to be 38.7 ± 1.0 nm and 40.4 ± 1.6 nm, respectively. No aggregation tendency was observable for γ-Fe_2O_3–PEGPEI over 12 h even in high ionic strength media. Furthermore, IC_{50} values were significantly increased by more than 10-fold when compared to γ-Fe_2O_3–PEI. Formulations exhibited r_2 relaxivities of high numerical value, namely around 160 $mM^{-1}\,s^{-1}$.

In summary, novel carrier systems composed of γ-Fe_2O_3–PEGPEI meet key quality requirements rendering them promising for biomedical applications, e.g. as MRI contrast agents.

1. Introduction

Magnetic iron oxide nanoparticles (IONPs) have met with increasing interest due to potential biomedical applications, amongst others in drug delivery (Cengelli et al., 2009; Chen et al., 2009), magnetic resonance imaging (MRI) (Howes et al., 2010; Li Calzi et al., 2009) and hyperthermia of tumors (Balivada et al., 2010). Recently, the design of such carrier systems has moved towards multifunctionality based on drug loaded IONP (Maeng et al., 2010; Santra et al., 2009) and more selectivity by the attachment of targeting ligands (Lee et al., 2010). In all cases, biocompatibility of IONP regarding immunogenicity and colloidal stability is of concern.

In general, surface coatings are necessary which influence aggregation behavior, colloidal stability in blood, cytotoxicity, and furthermore play a significant role in pharmacokinetics and biodistribution in the body (Gupta and Gupta, 2005). Stabilization strategies for magnetic iron oxide nanoparticles are mostly based on polymer coatings. Polymers investigated include crosslinked dextran, poly(lactic acid), poly(ethylene glycol), chitosan and polyvinyl alcohol (Laurent et al., 2008). Newer strategies concern amphiphilic polymers for phase transfer of IONP generated in organic solvents (Kim et al., 2010). Also, cationic polymers such as poly(ethylene imine) (PEI) have been used to stabilize IONP by adsorptive coating on numerous occasions (Thuenemann et al., 2006). Such IONP have been investigated in the context of multifunctional carriers allowing imaging and nucleic acid delivery (Huth et al., 2004; Arsianti et al., 2010), but also for targeting and imaging purposes (Chertok et al., 2010; Masotti et al., 2009).

One problem associated with PEI coated IONP is their lack of colloidal stability and cytotoxicity associated with the polymer. It has been demonstrated that such IONP tend to aggregate in certain cell culture media and in the presence of serum proteins (Petri-Fink et al., 2008). A potential strategy to overcome these problems could be the modification of PEI backbone with poly(ethylene glycol) (PEG), as PEG provides copolymers with increased stability, increased circulatory lives and lower toxicity (Jain and Jain, 2008). Only scant information is avail-

* Corresponding author. Tel.: +49 6421 28 25881; fax: +49 6421 28 27016.
E-mail address: kissel@staff.uni-marburg.de (T. Kissel).

0378-5173/$ – see front matter © 2011 Elsevier B.V. All rights reserved.
doi:10.1016/j.ijpharm.2010.12.046

able on IONP which were stabilized by copolymers of PEG and PEI (Zhou et al., 2009).

It was hypothesized that copolymers of the type poly(ethylene imine)-*g*-poly(ethylene glycol), PEGPEI could serve as coating agent for magnetic iron oxide nanoparticles leading to enhanced colloidal stability and reduced cytotoxicity due to PEG shielding effects. To verify these assumptions, γ-Fe_2O_3 nanoparticles were coated with PEGPEI using a straightforward manufacturing technique. These IONPs were compared with PEI coated nanoparticles to evaluate the effect of PEG shielding. IONPs were characterized with respect to physicochemical properties and composition. Moreover, colloidal stability and aggregation behavior was investigated, as well as cytotoxicity and contrast enhancement in MRI experiments.

2. Materials and methods

2.1. Materials

Iron(II)chloride tetrahydrate and iron(III)chloride hexahydrate were purchased from Sigma–Aldrich (Taufkirchen, Germany). Branched poly(ethylene imine) (PEI) with a molecular weight of 25,000 Da was a gift from BASF (Ludwigshafen, Germany). Block copolymers of the general composition PEI(25k)-*g*-PEG(20k)1, abbreviated as PEGPEI, were synthesized as previously described (Kissel et al., 1999). Synthesis procedures and dilution steps were carried out in ultra pure water (0.055 μS/cm, USF Seral, Seradest BETA 25 and Serapur DELTA UV/UF) unless otherwise stated. All other chemicals were obtained from commercial sources and used as received without further purification.

2.2. Preparation of γ-Fe_2O_3 nanoparticle cores

Iron oxide nanoparticles were prepared by an aqueous coprecipitation route adapted from the Massart process (Bee et al., 1995). Briefly, 2.6 mL of concentrated ammonia solution (25%) were slowly added to a 0.13 M slightly acidic solution of iron(III) chloride hexahydrate and iron(II)chloride tetrahydrate (molar ratio 2:1) of pH 2, until formation of a dark black slurry occurred. After collection with a permanent magnet and triple washing with ultra pure water, particles were refluxed in a mixture of nitric acid (10 mL, 2 M) and 0.34 M iron(III)nitrate nonahydrate at 90 °C for 30 min. The precipitate was collected by magnetic decantation and subsequently dispersed in water to yield a stable final suspension at pH 2.

Functionalized nanoparticles were generated by mixing the iron oxide suspensions with PEI or PEGPEI polymer solutions for 30 min at a defined mass ratio [Fe] to [PEI] of 1:2. Unbound polymer was removed by dialyzing the suspensions in multiple cycles against a 500-fold excess of ultra pure water, using Spectra/Por® membranes with MWCO 100,000 Da (Carl Roth, Karlsruhe, Germany).

2.3. Characterization of γ-Fe_2O_3 cores

2.3.1. Transmission electron microscopy

Size and morphology of γ-Fe_2O_3 cores were investigated using transmission electron microscopy (TEM). Suspension droplets were placed onto carbon-coated copper grids S160-3 (Plano, Wetzlar, Germany) and allowed to air dry. After insertion into the microscope JEM-3010 (Jeol Germany, Eching, Germany), pictures were taken at an acceleration voltage of 300 kV. Core dimensions were calculated by averaging at least 200 particle diameters using the ImageJ software.

2.3.2. X-ray diffraction

X-ray diffraction (XRD) patterns of naked iron oxide cores were recorded on a Panalytical X'Pert Pro powder diffractometer (Almelo, Netherlands) to characterize the crystallite type and structure of the material. For that purpose, particle suspensions were frozen at −80 °C for 1 h and lyophilized on a Christ Lyo Beta I (Osterode, Germany) at −40 °C and 0.05 mbar. After primary drying, samples were removed and desiccated thoroughly over dried silica gel, before being screened with the goniometer at 2θ angles from 20° to 80° at a stepwidth of 0.0131°.

2.3.3. Magnetization measurements

The dried samples were further investigated with regard to their expected superparamagnetic behavior. Small amounts of material were introduced into a Magnetic Property Measurement System MPMS® equipped with 5 T magnet (Quantum Design, San Diego, CA) using superconducting quantum interference device (SQUID) technology. Samples underwent a zero field-cooled field-cooled (zfc–fc) sweep from 5 to 350 K at a rate of 2 K/min and an external magnetic field strength of 50 and 500 Oe, respectively.

2.4. Characterization of polymer-coated nanoparticles

2.4.1. Dynamic light scattering

Hydrodynamic diameters of nanoparticles after polymer functionalization were assessed by dynamic light scattering (DLS) on a Zetasizer Nano ZS (Malvern Instruments, Herrenberg, Germany). Measurements were performed at 25 °C after appropriate dilution of the respective samples with ultra pure water to avoid multiscattering events. DTS v. 5.10-software was used to calculate both particle mean diameters from intensity-weighted distributions (Z-Ave) and distribution widths displayed as the polydispersity index (PDI).

2.4.2. Thermal gravimetric analysis and FT-IR spectroscopy

Investigations on the general and quantitative composition of polymer-coated iron oxide nanoparticles were carried out via thermal gravimetric analysis (TGA) and infrared spectroscopy (IR). In the course of the thermal analysis, lyophilized samples of iron oxide, pure PEI or PEGPEI and core–shell compounds thereof were tracked over a temperature range from 25 to 900 °C at a scan rate of 20 K/min under nitrogen atmosphere using a PerkinElmer TGA 7 assembly (Rodgau, Germany). Samples of similar type were also subjected to infrared wavenumber scans between 4000 and 400 cm^{-1} on a Bruker FT-IR spectrometer with Alpha Platinum ATR sampling module (Bruker Optics, Ettlingen, Germany).

2.5. Colloidal stability

The stability of the polymer-coated formulations was tested in a dual set of experiments. Firstly, change of particle diffusivity in different relevant media was examined over a time scale of 30 min. Herein, 10 μL of nanoparticle suspensions containing iron concentrations of 1 mg/mL were diluted 40-fold with one of the following agents: ultra pure water, sodium chloride 0.9% (w/v), fetal calf serum (FCS) of different concentrations or Dulbecco's modified eagle medium (DMEM) high glucose supplemented with 10% FCS and L-glutamine. Trends of diffusion coefficients over the half-hour period were monitored by dynamic light scattering on a Zetasizer Nano ZS at 25 °C with settings analogous to the section stated above for size measurements.

Secondly, the same formulations were analyzed at 37 °C for alterations in turbidity at 630 nm over 12 h with an Ultrospec 3000 spectrophotometer (Pharmacia Biotech, Vienna, Austria). Suspensions were mixed with the above-mentioned solutions in a 1:40 ratio and transmissions were recorded at given time points. Samples were stored in a thermal block at 37 °C throughout the whole experiment and redispersed prior to each measurement by vortexing.

2.6. Cell culture and trypan blue exclusion assay

Human lung adenocarcinoma cell line A549 was maintained in DMEM high glucose containing 10% FCS and L-glutamine without the addition of antibiotics in a humidified atmosphere at 37 °C and 8.5% CO_2. For the experiment, cells were seeded onto 24-well plates at a density of 60,000 per well. After awaiting adherent growth, culture medium was exchanged with DMEM supplemented with 5% FCS in order to avoid interference with the assay reagents. Immediately thereafter, the wells were incubated with increasing [Fe] concentrations of either iron oxide–PEI or iron oxide–PEGPEI for a period of 24 h. For the purpose of comparison, treatment with pure PEI was performed due to its well-known cytotoxic properties. Unmanipulated wells served as control. After 24 h, cells were washed twice with PBS to remove aggregated material and spiked with 20 μL of 0.4% trypan blue. 3 min after addition of the dye, magnified pictures of the respective wells were taken on a camera-equipped microscope. The percentage of cell viability was determined by inspecting at least 200 cells for lack or presence of intracellular blue color, as dead cells soak up the dye due to loss of membrane integrity.

2.7. MR relaxometry

Magnetic resonance imaging studies were carried out on a 7 T Bruker ClinScan 70/30 USR (Bruker BioSpin, Rheinstetten, Germany). Concentration series of polymer-functionalized iron oxide nanoparticles were placed into microcentrifuge cups to avoid artifacts from surrounding air. For measurements of transverse T_2 relaxation times, spin-echo multicontrast sequences were run at T_R values of 2000 ms, varying spin echo times T_E (10–150 ms with an increment of 10 ms), field of view 65 mm × 75 mm, matrix 112 × 128 and slice thickness 0.6 mm. Data quantification was achieved by evaluating DICOM images. T_2 maps were generated from the overlay of successive spin-echo images using a nonlinear monoexponential fitting of the signal intensity (SI) decay curve: $SI(t) = S_0 \exp(-t/T_2)$, where S_0 is the signal magnitude at equilibrium and t the particular echo time. Relaxation times T_2 and their reciprocal values, relaxation rates R_2 (=$1/T_2$) could therefore be derived by analyzing regions of interest (ROI) within the created maps.

Additionally, effective transverse relaxation times (T_2^*) were calculated from T_2^*-weighted images taken with the following settings: gradient–echo multicontrast with T_R 350 ms, multiple spin echo times T_E (2–5 ms), field of view 58 mm × 78 mm, matrix 96 × 128, slice thickness 0.5 mm. T_2^* values were obtained correspondingly by fitting the MRI signal intensities of the acquired maps versus echo times T_E.

2.8. Statistical analysis

Measurements were carried out in triplicate and data are presented as mean ± S.D. unless otherwise noted. For statistical testing, one-way ANOVA in conjunction with Bonferroni's post-t-test analysis were performed. Probability values of $p < 0.05$ were considered significant.

3. Results and discussion

3.1. Particle synthesis

Iron oxide nanoparticles prepared by the aqueous precipitation route (Bee et al., 1995) are generally of the maghemite (γ-Fe_2O_3) type, after mild oxidation of the intermediate modification magnetite (Fe_3O_4). Initial stabilization was conferred to the naked γ-Fe_2O_3 nanoparticles by electrostatic repulsion following peptization in acidic environment. Ammonia solution was added dropwise to the reaction mixture to induce a short burst of nucleation and controlled growth of IONP. Both parameters have been described to be essential for size uniformity according to the LaMer diagram (Beattle, 1989). Other factors determining particle size such as type, molarity and ratio of iron salts were kept constant throughout the whole manufacturing process. Mixing of iron oxide suspensions with polymer solutions yielded the formulations of interest, γ-Fe_2O_3–PEI and γ-Fe_2O_3–PEGPEI. The simplicity and lack of organic solvents generally render this coating procedure favorable for biological applications.

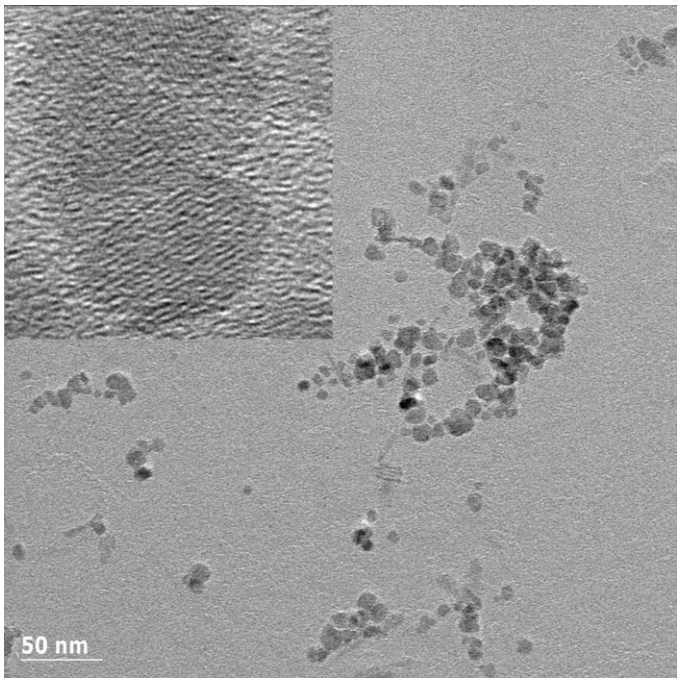

Fig. 1. Transmission electron micrographs on morphology of synthesized γ-Fe_2O_3 cores and crystallite structure at higher magnification (inset).

3.2. Physicochemical characterization

3.2.1. Size and morphology of γ-Fe_2O_3 cores

The maghemite cores depicted on TEM pictures (Fig. 1) were found to be irregularly shaped with an average diameter of 10.8 ± 3.0 nm and arranged in clusters because of their magnetic nature. Size values were obtained by averaging 200 core diameters, representing a number-weighted distribution pattern. Dynamic light scattering experiments showed considerably larger diameters due to the inclusion of regions of agglomeration and the analysis in intensity-weighted mode (data not shown). At very high magnifications, transmission electron micrographs revealed uniformly arranged planes inside the γ-Fe_2O_3 crystallite. Relatively wide size distribution and poor control of the shape of IONP are drawbacks generally observed with the aqueous coprecipitation route (Yu et al., 2004). However, distribution width is still in an acceptable range and the avoidance of organic solvents turns out to be beneficial for biomedical use. The high resolution images suggest an inverse spinel structure of the maghemite crystal lattice.

3.2.2. Crystal modification of synthesized iron oxide

Evidence of identity and crystal structure was further verified by X-ray diffraction patterns. Intensity signals appeared at defined scattering angles 2θ with the most prominent ones at 30.6°, 35.9°, 43.3°, 57.4° and 63.2° (Fig. 2). The Bragg peaks could be assigned to specific diffraction planes inside the maghemite lattice: (2 2 0), (3 1 1), (4 0 0), (5 1 1) and (4 4 0). The assembly of the diffraction

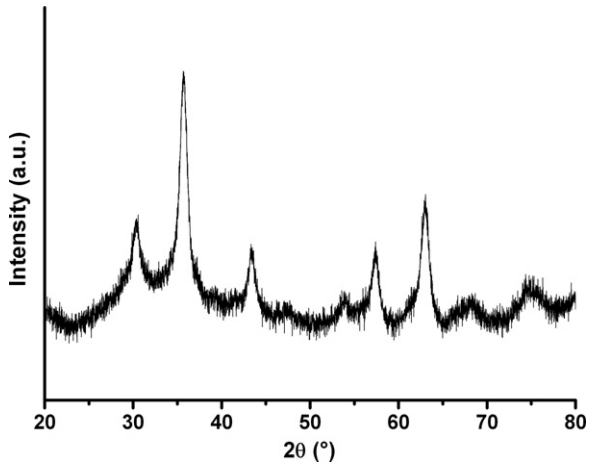

Fig. 2. XRD pattern of prepared iron oxide (γ-Fe_2O_3) nanoparticles indicative for inverse spinel structure. Signals are assignable to diffraction planes (2 2 0), (3 1 1), (4 0 0), (5 1 1) and (4 4 0) at 30.6°, 35.9°, 43.3°, 57.4° and 63.2°, respectively.

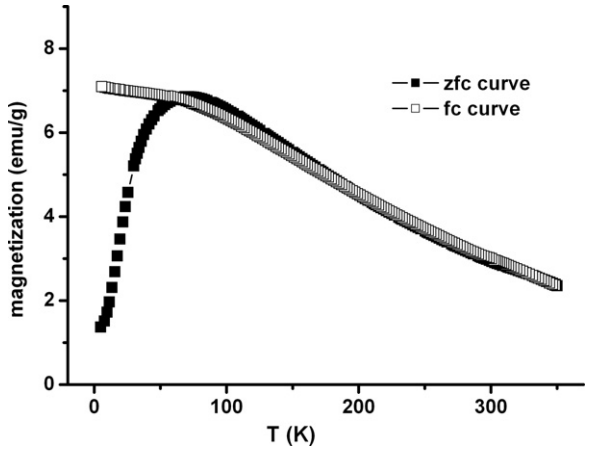

Fig. 3. Temperature-dependent magnetization of γ-Fe_2O_3 nanoparticles as obtained from zero field-cooled–field-cooled (zfc–fc) sweep at an external field strength of 50 Oe. Superparamagnetic limit is given by the maximum of the zfc curve, namely the blocking temperature T_B.

peaks is indicative for a cubic inverse spinel structure and conforms to maghemite/magnetite reference spectra due to the relative positions of signals (Si et al., 2004). In general, appearance of signals is regulated by the incident X-ray wavelength ($K_{\alpha1}$: 1.5406 nm, and $K_{\alpha2}$: 1.5444 nm). Distinguishability between the modifications γ-Fe_2O_3 and Fe_3O_4 is not possible due to the crystallographically isomorphous structures of both materials. Broadening of the peaks is caused by crystallite size and, to a minor extent, lattice strain (Zhang et al., 2003). By application of the Scherrer equation, which considers size contributions to peak broadening (Patterson, 1939), crystallite diameters were accessible. The formula is given by:

$$B = \frac{K\lambda}{L \cos q}$$

where B is the half-value width of respective Bragg peaks, λ is the applied X-ray wavelength, L is the diameter, θ is the Bragg angle and K is the shape-dependent Scherrer constant (set to 0.9). The calculated mean diameters of 10.3 ± 1.2 nm supported findings from transmission electron microscopy. The slight discrepancies between both methods are explained by the existence of thin amorphous layers on the surface of the iron oxide nanoparticles and the already mentioned lattice strain.

3.2.3. Superparamagnetism

Temperature-dependent magnetization measurements for naked iron oxide nanoparticles indicated the presence of a blocking temperature T_B of 75 K, visible in the zero field-cooled section, at an external field strength of 50 Oe (Fig. 3). Also, the rather broad distribution around the T_B maximum was clearly noticeable. Moreover, the blocking temperature shifted to lower values at 500 Oe and vanished completely at higher magnetic field strengths (data not shown). The appearance of T_B is an indicator for the superparamagnetic behavior of the prepared iron oxide species. Nanoscale magnetic particles possess a so-called blocking temperature as thermal limit that divides blocked and superparamagnetic state (Lu et al., 2007). Above this value, thermal energy exceeds anisotropy energy and leads to randomization of magnetic moments much faster than the experimental time scales. As seen here, the thermal energy input upon heating of the samples disturbs the systems initially leading to unblocking and alignment of magnetic moments with the external magnetic field. Thereafter, iron oxide nanoparticles drift into the superparamagnetic state characterized by randomization of magnetic vectors and decrease of magnetization. It can thus be concluded that the IONP are combining strong magnetic moments and paramagnetic behavior (superparamagnetism) which is of great importance for biomedical applications.

3.2.4. Hydrodynamic diameters of polymer-coated nanoparticles

All further physicochemical investigations were performed on the coated nanoparticle formulations after adsorptive layering with polymers. Particle sizes as measured by dynamic light scattering were found to be 38.7 ± 1.0 nm (γ-Fe_2O_3–PEI) and 40.4 ± 1.6 nm (γ-Fe_2O_3–PEGPEI), suggesting an increase in radii of 13–15 nm under the assumption that single iron oxide cores were layered with the respective polymers (Table 1). Polymer layer thickness is thus similar for both formulations despite PEGPEI displaying almost double molecular weight. The polydispersity indices (PDI) representing the widths of the fitted Gaussian distributions equaled to 0.212 ± 0.013 and 0.186 ± 0.018, respectively. As a result, these IONP had particle sizes smaller than those of the commercially available product Resovist® (60 nm) and may be designated as ultrasmall superparamagnetic iron oxide nanoparticles (USPIO). It has been shown earlier that poly(ethylene imine) can attach to very different surfaces within a broad pH range (Schneider et al., 2003). We assume that the binding mechanism of PEI onto maghemite is a combination of hydrogen bonding and dipolar interactions. The mentioned slight difference in polymer layer thickness suggests in our opinion the orientation of PEG molecules along the nanoparticle surface, thereby forming a protective shield in aqueous environment. Besides that, we observed an auto-regulation of the pH values after mixing iron oxide and polymer suspensions to numbers of 7.5–7.7, presumably evoked by the buffering capacity of the branched poly(ethylene imine) and its derivative PEGPEI. This enables an euhydric application of the formulation without further manipulations. So, despite its simplicity, this synthesis strategy permits the fabrication of small nanoparticulate carriers with relatively narrow size distributions at neutral pH.

Table 1
Physicochemical parameters of magnetic iron oxide nanoparticles.

	Size (nm)	r_2 (mM^{-1} s^{-1})	r_2* (mM^{-1} s^{-1})
γ-Fe_2O_3	10.8 ± 3.0[a]	n.d.	n.d.
γ-Fe_2O_3–PEI	38.7 ± 1.0[b]	163.2	249.1
γ-Fe_2O_3–PEGPEI	40.4 ± 1.6[b]	155.7	231.7

n.d.: not determined.
[a] As measured by TEM.
[b] As measured by DLS (mean ± S.D., n = 3).

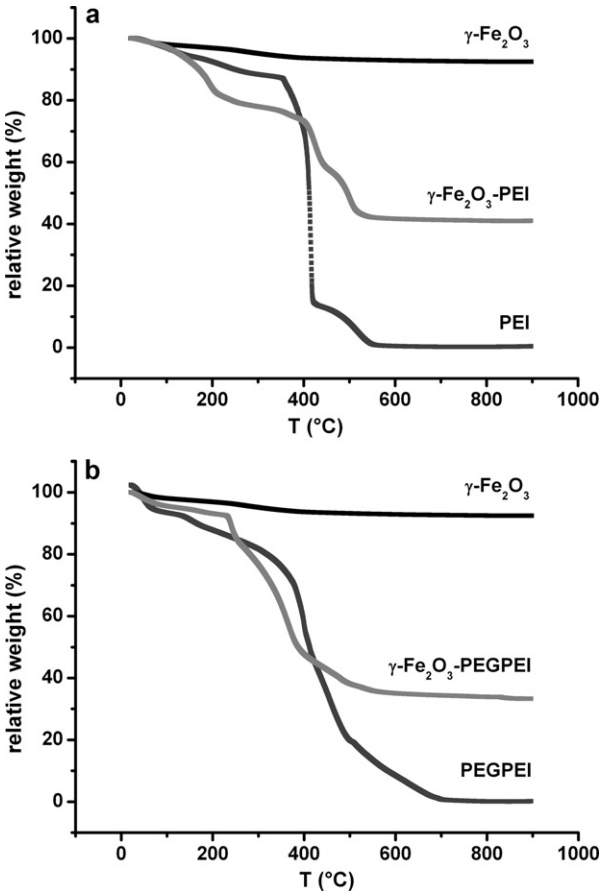

Fig. 4. Relative weight loss of hybrid nanoparticle systems (a) γ-Fe_2O_3–PEI and (b) γ-Fe_2O_3–PEGPEI upon heating to 900 °C (TGA). Respective curves for naked γ-Fe_2O_3 cores and pure polymers were taken for comparison reasons.

3.2.5. Composition of polymer-coated nanoparticles

In additional experiments, the relative composition of the hybrid particles, consisting of an inorganic iron oxide core and an organic polymer shell, was assessed by thermal analysis and IR spectrometry. Thermograms revealed a degradation onset for pure PEI at 370 °C and a biphasic degradation process for PEGPEI. The curves for the hybrid nanoparticles showed analogous patterns and remainder of the inorganic iron oxide cores at high temperatures (Fig. 4a and b). Due to apparent minimum water residues in the samples, an absolute quantification of polymer contribution to the overall particle mass was difficult but estimated to be 55% in the case of PEI and 65% for PEGPEI. The degradation temperature values obtained were in good accordance with results from earlier studies (Petersen et al., 2002a). Furthermore, it became obvious that almost all polymer applied during the layering process of maghemite nanoparticles is bound to the surface (maximum mass fraction PEI 59% and PEGPEI 72%). Only a small percentage got washed out during dialysis purification of the batches. Further evidence for the qualitative assembly of the hybrid nanoparticles was gained by infrared spectra, for clarity only data for the γ-Fe_2O_3–PEI type are shown. Vibration signals originating from the Fe–O bond were found at wavenumbers of 630, 585 and 440 cm^{-1} and coexisted for both pure maghemite and γ-Fe_2O_3–PEI nanoparticles (Fig. 5). Moreover, characteristic bands for poly(ethylene imine) like the N–H stretch at 3500–3300 cm^{-1} were recorded and coincided with those of hybrid particles. Others reported that finite-size effects in nanoparticulate maghemite cause splitting of the Fe-O ν_1 band to values above 570 cm^{-1} and shifting of the ν_2 band (375 cm^{-1}) to higher wavenumbers (Yamaura et al., 2004).

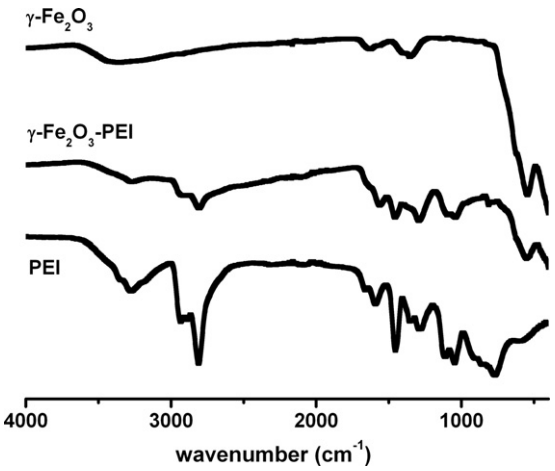

Fig. 5. Infrared wavenumber scans for lyophilized γ-Fe_2O_3–PEI and its singular components. Spectra were arranged on top of each other due to clarity purposes.

3.3. Colloidal stability in different media

Diffusion coefficients of formulations γ-Fe_2O_3–PEI and γ-Fe_2O_3–PEGPEI in various media as calculated from the DLS auto-correlation function were recorded to identify alterations in overall particle size. The changes were most pronounced for γ-Fe_2O_3–PEI in supplemented cell medium DMEM with a 65% decrease of diffusion coefficients after 30 min, while dispersion of both formulations in saline or fetal calf serum left the particle diffusivity rather unchanged with a minor exception for very high protein levels in FCS 90% (Fig. 6a and b). Turbidity measurements over 12 h generally confirmed these findings as the decay of transmission indicating aggregation of nanoparticles was found to be most distinct for γ-Fe_2O_3–PEI in DMEM 10% FCS (Fig. 6c and d), also macroscopically observable by a complete loss of transparency.

The results suggest that adsorption of serum components did not induce detrimental effects on stability of polymer-coated iron oxide nanoparticle systems, as seen by the constancy of relative diffusion coefficients. However, absolute sizes after protein adsorption were found to be slightly enhanced for the γ-Fe_2O_3–PEI type, hinting at facilitated and increased attachment of the protein fraction. When additionally introduced into a high ionic strength environment like DMEM, these carriers begin to precipitate massively, presumably due to shrinkage of the electrical double layers and loss of repulsive shielding between the particles. The improved performance of γ-Fe_2O_3–PEGPEI (in DMEM 10% FCS) is assumed to be caused by an effective reduction in absolute protein adsorption levels, thus retaining individuality of the nanoparticles, and may be attributed in large part to the presence of surface PEG moieties. PEG coatings have been shown to prevent protein fouling and to provide steric hindrance suppressing aggregation (Fang et al., 2009). As cell medium DMEM 10% FCS has a similar ionic composition to simulated body fluid and equals human blood serum assembly, results are promising for a possible *in vivo* application of PEGPEI-modified nanoparticles. On the one hand, these particles can evade rapid sequestration in MPS organs due to their small size and stability (Owens and Peppas, 2006), on the other hand iron oxide pegylation offers possibly the beneficial effect of reduced protein opsonization *in vivo*. Through the synergistic combination of these mechanisms, the blood circulation half-lives of the carriers are supposed to be greatly enhanced, and hence the access to deeper compartments is facilitated (Corot et al., 2006).

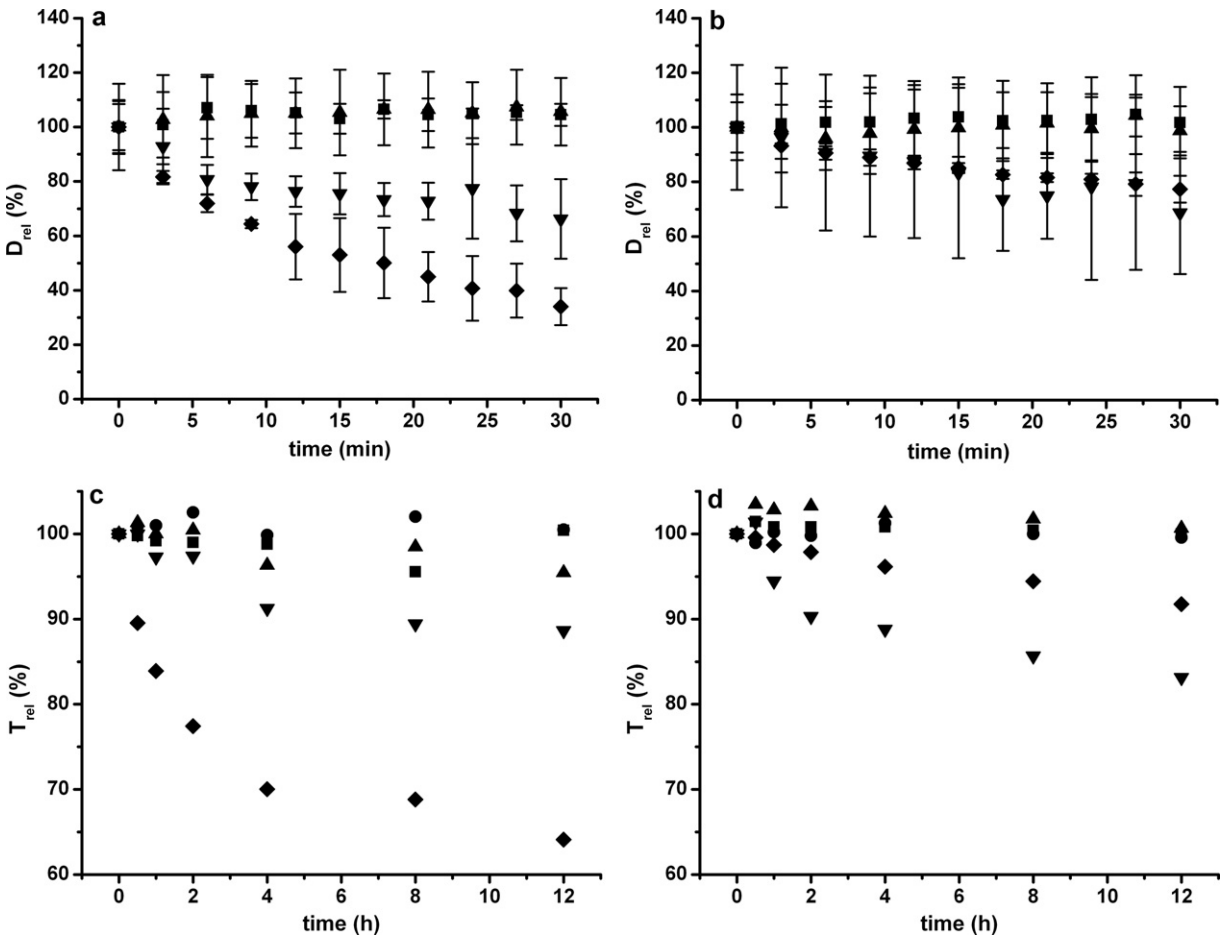

Fig. 6. Colloidal stability of nanoparticle formulations in NaCl 0.9% (■), FCS 10% (▲), FCS 90% (▼) and DMEM supplemented with 10% FCS (♦) as measured by changes of relative diffusion coefficients D_{rel} and relative transmissions T_{rel} over time. Initial values were set to 100%. Course of D_{rel} was monitored for (a) γ-Fe_2O_3–PEI and (b) γ-Fe_2O_3–PEGPEI nanoparticles ($n = 3$) in the different media. Graphs (c) and (d) show transmission data at 630 nm for γ-Fe_2O_3–PEI and γ-Fe_2O_3–PEGPEI, respectively.

3.4. Cytotoxicity assessment

A549 cell viability profiles after incubation with nanoparticulate [Fe] amounts of 0.1–100 μg/mL were sigmoidally fitted and yielded IC_{50} values of 6.8 and 160 μg/mL [Fe] for γ-Fe_2O_3–PEI and γ-Fe_2O_3–PEGPEI, respectively (data not shown). Due to the fact that cytotoxicity of hybrid iron oxide nanoparticles in the applied concentration range is caused to a major extent by their polymeric coatings (Hussain et al., 2005), incubation concentrations were recalculated and standardized to polymer molarities of either PEI or PEGPEI, and viability curves were replotted for comparison purposes (Fig. 7). For example, the incubation amount of 10 μg/mL [Fe] equals 14.3 μg/mL of γ-Fe_2O_3 and, given the findings from TGA analysis where hybrid γ-Fe_2O_3–PEI nanoparticles were found to contain 60% of polymer, subsequently 21.5 μg/mL or 0.86 μM of PEI. Thereafter, it could be clearly seen that poly(ethylene imine) layered on iron oxide particles exhibited cytotoxicity comparable to free PEI polymer while PEGPEI created these effects only when applied at an almost 20-fold amount. Despite the implemented approximation, the informative value of the chosen display is in our opinion higher as for standard depictions plotting viability versus iron concentration. The known cytotoxicity of poly(ethylene imine) originates from its strong cationic character which is responsible for inducing defects into lipid bilayers (Leroueil et al., 2008). Shielding of cytotoxicity has been reported to be brought about by covalent attachment of poly(ethylene glycol) to harmful polymers like PEI. However, the massive reduction in cytotoxicity seen here outscores findings for free PEI(25k)-*g*-PEG(20k)1 polymer (Debus et al., 2010) and polyplexes where decrease of cell-detrimental effects upon pegylation was not that pronounced (Petersen et al., 2002b). Also, modification of PEI 25 kDa was shown to reduce cytotoxic and oxidative stress most effectively at high degrees of PEGylation and low PEG chain lengths (Beyerle et al., 2010). We explain the different behavior by the fact that PEG moieties on the surface of iron

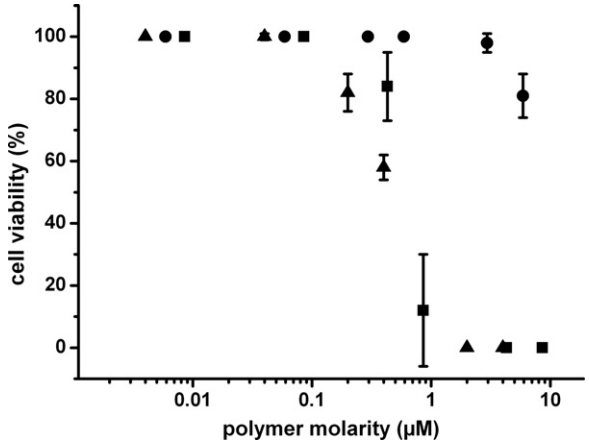

Fig. 7. A549 cell viability as observed by trypan blue exclusion assay after incubation with dilutions of PEI 25k (▲), γ-Fe_2O_3–PEI (■) and γ-Fe_2O_3–PEGPEI (●). Values are plotted against polymer fractions of each formulation. IC_{50} numbers were accessible by sigmoidal fitting of the curves.

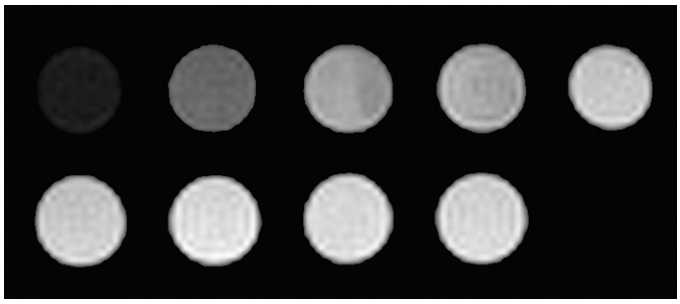

Fig. 8. T_2^*-weighted image of γ-Fe_2O_3–PEI nanoparticle suspensions with [Fe] concentrations of 100, 50, 30, 20, 10, 5, 2, 1 and 0.1 μg/mL (top left to bottom right).

oxide nanoparticles are mainly directed towards the surrounding medium thereby efficiently contributing to the shielding of these systems, whereas polyplexes hide large parts thereof on the inside. Fetal calf serum concentration was reduced to 5% prior to incubation experiments in order to minimize masking effects by proteins (Schulze et al., 2008).

3.5. Potential of IONP as MRI contrast agent

Relaxivities r_2 and r_2^* were accessible by measuring relaxation times for concentration series of the formulations γ-Fe_2O_3–PEI and γ-Fe_2O_3–PEGPEI via the general equation:

$$\frac{1}{T_2^*} = \frac{1}{T_{\text{init.}}} + r_2^* C$$

where $T_{\text{init.}}$ represents the initial relaxation time, and T_2 or T_2^* are the relaxation times determined for [Fe] concentrations C. Experimental values for r_2 at a magnetic field strength of 7 T accounted to 163.2 and 155.7 $mM^{-1}\,s^{-1}$ for γ-Fe_2O_3–PEI and γ-Fe_2O_3–PEGPEI, respectively (Table 1). Gradient-echo T_2^* images of linearly arranged concentration series of γ-Fe_2O_3–PEI suspensions revealed loss of signal decay with decreasing iron concentrations, visible by transient brightening of the respective microcentrifuge tubes (Fig. 8). This phenomenon is caused by the significant enhancement of transverse proton relaxation in the vicinity of areas containing magnetic iron oxide, thus leading to quick fading of MR signals. As the coating thickness negatively affects the performance of magnetic nanoparticles, the slightly higher r_2 and r_2^* values for γ-Fe_2O_3–PEI particles can be attributed to their lower polymer fraction. However, the calculated r_2 relaxivities are a measure for the efficiency of contrast agents and were found to be superior to most marketed products (Casula et al., 2010). Taken together, the results prove the possibility of applying the formulations as MR contrast agents, e.g. for cell tracking where accelerated uptake behavior mediated by positive surface charges would increase the degree of cellular labeling.

4. Conclusions

An interesting alternative to current polymer candidates for coating of iron oxide nanoparticles was suggested to be poly(ethylene imine)-*g*-poly(ethylene glycol) (PEGPEI), representing in our opinion an advancement of pure poly(ethylene imine) in terms of colloidal stability and cytotoxicity due to introduced PEG shielding moieties. We generated a novel magnetic carrier system based on the assembly of PEGPEI and iron oxide nanoparticles which meets the premium requirements for biomedical applications, amongst these small size, narrow size distribution and superparamagnetism. Despite the simplicity of the synthesis procedure, γ-Fe_2O_3–PEGPEI particle systems displayed good colloidal stability over long-term range when suspended in critical cell media. Moreover, particle-associated toxicity was significantly reduced in contrast to γ-Fe_2O_3–PEI due to introduction of hydrophilic PEG groups to the polymer backbone. Relaxometric data underlined the general ability to enhance contrast in magnetic resonance imaging. The findings confirm the assumptions of increased stability and reduced cytotoxicity after nanoparticle coating with PEGPEI. Given the mentioned results, iron oxide–PEGPEI nanoparticles possess great potential for biomedical applications. Especially the use of these carriers for cell tracking purposes is envisioned where sufficient intracellular accumulation and concurrent absence of toxicity are needed. These effects are supposed to be balanced well for γ-Fe_2O_3–PEGPEI, but need to be investigated in further studies.

Acknowledgements

The authors thank Maximilian Voelker from the Department of Diagnostic Radiology, Marburg, Germany for assistance with MR measurements and Eva Mohr for support in cell culture questions.

References

Arsianti, M., Lim, M., Marquis, C.P., Amal, R., 2010. Assembly of polyethylenimine-based magnetic iron oxide vectors: insights into gene delivery. Langmuir 26, 7314–7326.
Balivada, S., Rachakatla, R.S., Wang, H., Samarakoon, T.N., Dani, R.K., Pyle, M., Kroh, F.O., Walker, B., Leaym, X., Koper, O.B., Tamura, M., Chikan, V., Bossmann, S.H., Troyer, D.L., 2010. A/C magnetic hyperthermia of melanoma mediated by iron(0)/iron oxide core/shell magnetic nanoparticles: a mouse study. BMC Cancer 10, 119–127.
Beattle, J.K., 1989. Monodisperse colloids of transition metal and lanthanide compounds. Pure Appl. Chem. 61, 937–941.
Bee, A., Massart, R., Neveu, S., 1995. Synthesis of very fine maghemite particles. J. Magn. Magn. Mater. 149, 6–9.
Beyerle, A., Merkel, O., Stoeger, T., Kissel, T., 2010. PEGylation affects cytotoxicity and cell-compatibility of poly(ethylene imine) for lung application: structure–function relationships. Toxicol. Appl. Pharmacol. 242, 146–154.
Casula, M.F., Floris, P., Innocenti, C., Lascialfari, A., Marinone, M., Corti, M., Sperling, R.A., Parak, W.J., Sangregorio, C., 2010. Magnetic resonance imaging contrast agents based on iron oxide superparamagnetic ferrofluids. Chem. Mater. 22, 1739–1748.
Cengelli, F., Grzyb, J.A., Montoro, A., Hofmann, H., Hanessian, S., Juillerat-Jeanneret, L., 2009. Surface-functionalized ultrasmall superparamagnetic nanoparticles as magnetic delivery vectors for camptothecin. ChemMedChem 4, 988–997.
Chen, B., Lai, B., Cheng, J., Xia, G., Gao, F., Xu, W., Ding, J., Gao, C., Sun, X., Xu, C., Chen, W., Chen, N., Liu, L., Li, X., Wang, X., 2009. Daunorubicin-loaded magnetic nanoparticles of Fe_3O_4 overcome multidrug resistance and induce apoptosis of K562-n/VCR cells in vivo. Int. J. Nanomed. 4, 201–208.
Chertok, B., David, A.E., Yang, V.C., 2010. Polyethyleneimine-modified iron oxide nanoparticles for brain tumor drug delivery using magnetic targeting and intracarotid administration. Biomaterials 31, 6317–6324.
Corot, C., Robert, P., Idee, J.-M., Port, M., 2006. Recent advances in iron oxide nanocrystal technology for medical imaging. Adv. Drug Deliv. Rev. 58, 1471–1504.
Debus, H., Baumhof, P., Probst, J., Kissel, T., 2010. Delivery of messenger RNA using poly(ethylene imine)–poly(ethylene glycol)-copolymer blends for polyplex formation: biophysical characterization and in vitro transfection properties. J. Control. Release 148, 334–343.
Fang, C., Bhattarai, N., Sun, C., Zhang, M., 2009. Functionalized nanoparticles with long-term stability in biological media. Small 5, 1637–1641.
Gupta, A.K., Gupta, M., 2005. Synthesis and surface engineering of iron oxide nanoparticles for biomedical applications. Biomaterials 26, 3995–4021.
Howes, P., Green, M., Bowers, A., Parker, D., Varma, G., Kallumadil, M., Hughes, M., Warley, A., Brain, A., Botnar, R., 2010. Magnetic conjugated polymer nanoparticles as bimodal imaging agents. J. Am. Chem. Soc. 132, 9833–9842.
Hussain, S.M., Hess, K.L., Gearhart, J.M., Geiss, K.T., Schlager, J.J., 2005. In vitro toxicity of nanoparticles in BRL 3A rat liver cells. Toxicol. In Vitro 19, 975–983.
Huth, S., Lausier, J., Gersting Soeren, W., Rudolph, C., Plank, C., Welsch, U., Rosenecker, J., 2004. Insights into the mechanism of magnetofection using PEI-based magnetofectins for gene transfer. J. Gene Med. 6, 923–936.
Jain, A., Jain, S.K., 2008. PEGylation: an approach fro drug delivery. A review. Crit. Rev. Ther. Drug Carrier Syst. 25, 403–447.
Kim, M., Jung, J., Lee, J., Na, K., Park, S., Hyun, J., 2010. Amphiphilic comb like polymers enhance the colloidal stability of Fe_3O_4 nanoparticles. Colloids Surf. B 76, 236–240.
Kissel, T., Petersen, H., Fischer, D., Kunath, K., von Harpe, A., 1999. Cationic Block Copolymers, WO/2001/005875.
Laurent, S., Forge, D., Port, M., Roch, A., Robic, C., Vander Elst, L., Muller, R.N., 2008. Magnetic iron oxide nanoparticles: synthesis, stabilization, vectorization,

physicochemical characterizations, and biological applications. Chem. Rev. 108, 2064–2110.
Lee, C.-M., Jeong, H.-J., Cheong, S.-J., Kim, E.-M., Kim, D.W., Lim, S.T., Sohn, M.-H., 2010. Prostate cancer-targeted imaging using magnetofluorescent polymeric nanoparticles functionalized with bombesin. Pharm. Res. 27, 712–721.
Leroueil, P.R., Berry, S.A., Duthie, K., Han, G., Rotello, V.M., McNerny, D.Q., Baker Jr., J.R., Orr, B.G., Banaszak Holl, M.M., 2008. Wide varieties of cationic nanoparticles induce defects in supported lipid bilayers. Nano Lett. 8, 420–424.
Li Calzi, S., Kent, D.L., Chang, K.-H., Padgett, K.R., Afzal, A., Chandra, S.B., Caballero, S., English, D., Garlington, W., Hiscott, P.S., Sheridan, C.M., Grant, M.B., Forder, J.R., 2009. Labeling of stem cells with monocrystalline iron oxide for tracking and localization by magnetic resonance imaging. Microvasc. Res. 78, 132–139.
Lu, A.H., Salabas, E.L., Schueth, F., 2007. Magnetic nanoparticles: synthesis, protection, functionalization, and application. Angew. Chem. Int. Ed. 46, 1222–1244.
Maeng, J.H., Lee, D.-H., Jung, K.H., Bae, Y.-H., Park, I.-S., Jeong, S., Jeon, Y.-S., Shim, C.-K., Kim, W., Kim, J., Lee, J., Lee, Y.-M., Kim, J.-H., Kim, W.-H., Hong, S.-S., 2010. Multifunctional doxorubicin loaded superparamagnetic iron oxide nanoparticles for chemotherapy and magnetic resonance imaging in liver cancer. Biomaterials 31, 4995–5006.
Masotti, A., Pitta, A., Ortaggi, G., Corti, M., Innocenti, C., Lascialfari, A., Marinone, M., Marzola, P., Daducci, A., Sbarbati, A., Micotti, E., Orsini, F., Poletti, G., Sangregorio, C., 2009. Synthesis and characterization of polyethylenimine-based iron oxide composites as novel contrast agents for MRI. Magn. Reson. Mater. Phys.: Biol. Med. 22, 77–87.
Owens, D.E., Peppas, N.A., 2006. Opsonization, biodistribution, and pharmacokinetics of polymeric nanoparticles. Int. J. Pharm. 307, 93–102.
Patterson, A.L., 1939. The Scherrer formula for X-ray particle-size determination. Phys. Rev. 56, 978–982.
Petersen, H., Fechner, P.M., Fischer, D., Kissel, T., 2002a. Synthesis characterization, and biocompatibility of polyethylenimine-graft-poly(ethylene glycol) block copolymers. Macromolecules 35, 6867–6874.
Petersen, H., Fechner, P.M., Martin, A.L., Kunath, K., Stolnik, S., Roberts, C.J., Fischer, D., Davies, M.C., Kissel, T., 2002b. Polyethylenimine-graft-poly(ethylene glycol) copolymers: influence of copolymer block structure on DNA complexation and biological activities as gene delivery system. Bioconjug. Chem. 13, 845–854.
Petri-Fink, A., Steitz, B., Finka, A., Salaklang, J., Hofmann, H., 2008. Effect of cell media on polymer coated superparamagnetic iron oxide nanoparticles (SPIONs): colloidal stability, cytotoxicity, and cellular uptake studies. Eur. J. Pharm. Biopharm. 68, 129–137.
Santra, S., Kaittanis, C., Grimm, J., Perez, J.M., 2009. Drug/dye-loaded multifunctional iron oxide nanoparticles for combined targeted cancer therapy and dual optical/magnetic resonance imaging. Small 5, 1862–1868.
Schneider, M., Brinkmann, M., Moehwald, H., 2003. Adsorption of polyethylenimine on graphite: an atomic force microscopy study. Macromolecules 36, 9510–9518.
Schulze, C., Kroll, A., Lehr, C.-M., Schaefer, U.F., Becker, K., Schnekenburger, J., Isfort, C.S., Landsiedel, R., Wohlleben, W., 2008. Not ready to use – overcoming pitfalls when dispersing nanoparticles in physiological media. Nanotoxicology 2, 51–61.
Si, S., Kotal, A., Mandal, T.K., Giri, S., Nakamura, H., Kohara, T., 2004. Size-controlled synthesis of magnetite nanoparticles in the presence of polyelectrolytes. Chem. Mater. 16, 3489–3496.
Thuenemann, A.F., Schuett, D., Kaufner, L., Pison, U., Moehwald, H., 2006. Maghemite nanoparticles protectively coated with poly(ethylene imine) and poly(ethylene oxide)-block-poly(glutamic acid). Langmuir 22, 2351–2357.
Yamaura, M., Camilo, R.L., Sampaio, L.C., Macedo, M.A., Nakamura, M., Toma, H.E., 2004. Preparation and characterization of (3-aminopropyl)triethoxysilane-coated magnetite nanoparticles. J. Magn. Magn. Mater. 279, 210–217.
Yu, W.W., Falkner, J.C., Yavuz, C.T., Colvin, V.L., 2004. Synthesis of monodisperse iron oxide nanocrystals by thermal decomposition of iron carboxylate salts. Chem. Commun. (Camb.), 2306–2307.
Zhang, H., Gilbert, B., Huang, F., Banfield, J.F., 2003. Water-driven structure transformation in nanoparticles at room temperature. Nature (Lond.) 424, 1025–1029.
Zhou, J.H., Huang, L., Wang, W.W., Pang, J., Zou, Y., Shuai, X.T., Gao, X., 2009. Prostate cancer targeted MRI nanoprobe based on superparamagnetic iron oxide and copolymer of poly(ethylene glycol) and polyethyleneimin. Chin. Sci. Bull. 54, 3137–3146.